Bull. Chem. Soc. Ethiop. **2024**, 38(2), 297-304.
DOI: https://dx.doi.org/10.4314/bcse.v38i2.2

ISSN 1011-3924
Printed in Ethiopia
Online ISSN 1726-801X

EXPLORING THE EFFECT OF CHROMIUM DOPING ON ELECTRONIC PROPERTIES, HALF-METALLIC AND FERROMAGNETISM ON ALSB DMS COMPOUND THROUGH FIRST-PRINCIPLES CALCULATIONS

Zakaria El Merzouki[1], Elhassan Benhsin[2*] and Mohammed Cherraj[1]

[1]Team of Modelling and Simulating in Mechanics and Energetics Energy Research Centre, Faculty of Sciences, Mohamed V University, B.P. 1014, Rabat, Morocco
[2]Laboratoire de Chimie Appliquée des Matériaux, Centre des Sciences des Matériaux, Faculty of Sciences, Mohammed V University in Rabat, Avenue Ibn Battouta, BP 1014, Rabat, Morocco

(Received March 29, 2023; Revised November 6, 2023; Accepted November 7, 2023)

ABSTRACT. With the aim of improving and investigating magnetocaloric insights for spintronic applications, we investigated the electronic structure of Cr-doped AlSb compounds via first-principles calculations using the KKR-CPA-DFT method. Here, we investigated the stability of alloy materials as a function of magnetic contamination. A stable semimetallic ferromagnetic phase can be obtained by introducing the Cr element into AlSb, which is inherent in nonmagnetic semiconductors. The total magnetic moment of the doped material changes from 0.1167 μB to 0.716 μB for 4% and 25% Cr, respectively. Curie temperature changed to 740 K at 25% Cr concentration.

KEY WORDS: Magnetic materials, Semiconductor, Alloys, Impurities

INTRODUCTION

Spin electronics is a field that emphasizes spin as an information vector. Applications in this area are widespread today, although spintronic devices can be found in hard disk read heads, magnetic non-volatile random access memories (MRAM), and magnetic sensors, but their primary application is information storage. Moving to information processing via more complex spin-logic architectures requires platforms that can inject, propagate, detect, and potentially manipulate spin information at macroscopic distances [1-3].

Spintronic materials are an integral part of modern technology. Due to its unique characteristics and sophisticated breeding methods, it is widely used in the electronics industry. In this context, Al-Sb alloys have been introduced into spintronics, supported by previously obtained promising results [4, 5].

Aluminum antimonide (Al-Sb) is of renewed interest in a variety of applications ranging from ionizing radiation detection to microelectronics and optoelectronics. For gamma-ray detection, Al-Sb materials are particularly promising as novel materials that can be detected with high energy resolution at room temperature. This was later attributed to the indirect bandgap of 1.6 eV in the Al-Sb system, the high atomic number of Sb, potentially large electrons, and hole motions up to several hundred cm $V^{-1}.s^{-1}$ is due to room temperature [6].

Indeed, there are limited theoretical and experimental reports on the physical properties of dilute AlSb-based magnetic semiconductors (SGs). Many efforts have been made to improve the performance of Sb-rich materials. For example, adding Si, Al, O, and W to Sb-rich materials can effectively improve thermal stability and material grain homogeneity [7]. AlSb, which is less common than GaAs in III-V semiconductors, is called the 6.1 Å family and has indirect and direct band gaps of 1.6 eV and 2.6 eV, respectively [8]. Potential applications in the field of spintronics, electro-optical and electronic devices [9], as well as high-energy solar cells, p-n junction diodes and transistors [9-11]. This compound has been used, for example, as a high-temperature

*Corresponding author. E-mail: h.benhsina@gmail.com

semiconductor material [9, 12], as an anode candidate for sodium/lithium-ion batteries, and is also promising as a photon detector [8, 13]. In microelectronics, AlSb and its related alloys are used in advanced field effect transistor designs that promise faster switching speeds and lower power consumption than silicon devices. This work is part of a larger effort to understand the fundamental microscopic limits of performance of this semiconductor material and others. Our major findings in this work are that the dominant native defects in AlSb are aluminum interstitials, antimony anti-sites, and aluminum vacancies, depending on chemical environment and doping. Transition metals and rare element are the most important and studied compounds [14-16].

The intrinsic defect and charge carrier concentrations of the impurity-free material are calculated by coherently solving the charge neutrality equation. We find that the material without impurities is n-conducting at a finite temperature. In this investigation, chromium (Cr) was introduced as a dopant into the phase change material AlSb. The resulting material, $Al_{(1-x)}Cr_xSb$, underwent thorough characterization involving assessments of thermal stability, crystal structure, and electrical performance. It was observed that higher concentrations of chromium led to enhanced thermal stability. The study identified an optimal composition that exhibited improved particle uniformity.

The aim of this work was to evaluate the effect of doping on the stability of DMS. To this end, first-principles calculations using the KKR-CPA-DFT method were performed to predict and clarify the magnetic and electronic properties of dilute magnetic semiconductors based on chromium-doped Al-Sb.

COMPUTATIONAL METHOD AND CRYSTAL STRUCTURE

The Korringa-Kohn-Rostoker coherent potential approximation (KKR-CPA) method was used to calculate the structural, electronic and magnetic properties of this system [17, 18]. The calculation uses density functional theory (DFT) [19, 20] and is implemented in the program package MACHIKANEYAMA2002v09 [21]. Akai *et al.* have developed his KKR-CPA method dealing with transition metal (TM) alloys [22].

In this method, the so-called outer and inner wavefunctions of the extended sphere are expanded into atom-centered extended spherical waves, which are Hankel functions or numerical solutions to the Schrödinger equation. Additional extended spherical waves were placed at carefully selected interstitials to optimize the basic set.

The selection and expansion radii of these sites were determined automatically using the sphere geometry optimization (SGO) algorithm. Self-consistency was achieved by a highly efficient convergence acceleration algorithm. Brillouin zone (BZ) integration was performed with an increasing number of k points (6 6 8) to ensure convergence of results on the spatial grid. The geometry is fully relaxed using Hermann-Feynman forces and total energy. For the self-consistent method, the convergence criterion is set to 10^{-8} eV and the charge difference DQ = 108 C between two successive iterations.

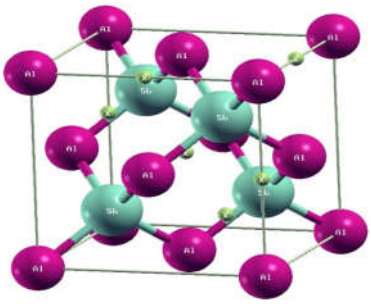

Figure 1. Structure of AlSb alloy.

The alloy compound AlSb has a cubic crystal structure with space group symmetry F-43m No. 216 and cell parameter a = 6.2337, with Al and Sb atoms at (0, 0, 0) and (1/4, 1/4, 1/4) position. Figure 1 shows the structure of pure AlSb optimized in this work using first principal component calculations.

RESULTS AND DISCUSSION

Insights into the electronic structure and magnetism of AlSb doped with a single impurity Cr are explored by the Korringa-Kohn-Rostoker coherence potential approximation (KKR-CPA). First, we investigated the properties of intrinsic AlSb for comparison. Figure 2 shows the total density of states (TDOS) and orbital projected density of states (PDOS) for pure AlSb calculated within the GGA approximation.

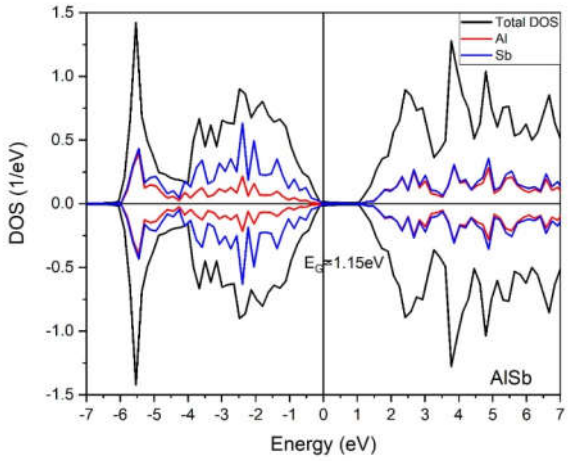

Figure 2. Total density of state (TDOS) and orbital projected density of state (PDOS) of pure AlSb.

A previous study [23] using a pulsed laser deposition (PLD) technique measured the band gaps of AlSb films to be 1.56 and 1.66 eV, which is larger than the estimated value of 1.15 eV. This discrepancy between experimental and calculated values is mainly due to known limitations of the exchange-correlation functional in DFT calculations [20]. Moreover, the high symmetry of the up-spin and down-spin density of states (DOS) and the zero total magnetic moment indicate that pure AlSb is a non-magnetic crystal.

Aluminium is replaced with various concentrations of chromium to induce magnetic properties in the inherent AlSb. Increasing the amount of chromium introduced on the Al sites changes both the electrical and magnetic behaviour of the material. Chromium atoms have more electrons than aluminium atoms and behave like additional donors, creating Cr 3d states around the gap energy. These states are responsible for bandgap narrowing and may act as traps for electron-hole pairs.

This project investigates alloys with different chromium contents with the formula $Al_{1-x}Cr_xSb$, where x is from 4% to 20%. The TDOS and PDOS curves shown in Figure 2 show that the spins are nearly 100% polarized. The down-spin channel has an indirect bandgap that lies between the valence band maximum and the conduction band minimum. Conversely, a new peak observed only in the spin-up state originates from chromium (Cr-3d) spin-up electrons appearing near the

Fermi energy (Ef). This indicates that the connection has become magnetic and the top-bottom spin symmetry has been broken, but its stability has not yet been determined. The creation of localized moments in Cr is responsible for magnetism.

The states consisting of Cr-3d, Al-p, and Sb-p near the Fermi level are crucial for half-metallic behavior and FM stability. The high hybridization between Cr-3d and Sb-p at the Fermi level explains why the double exchange mechanism is responsible for the magnetism and stability of FM states.

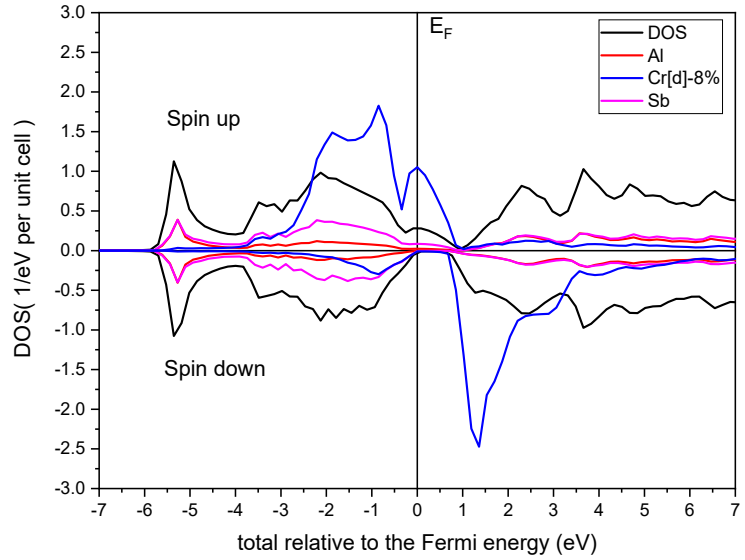

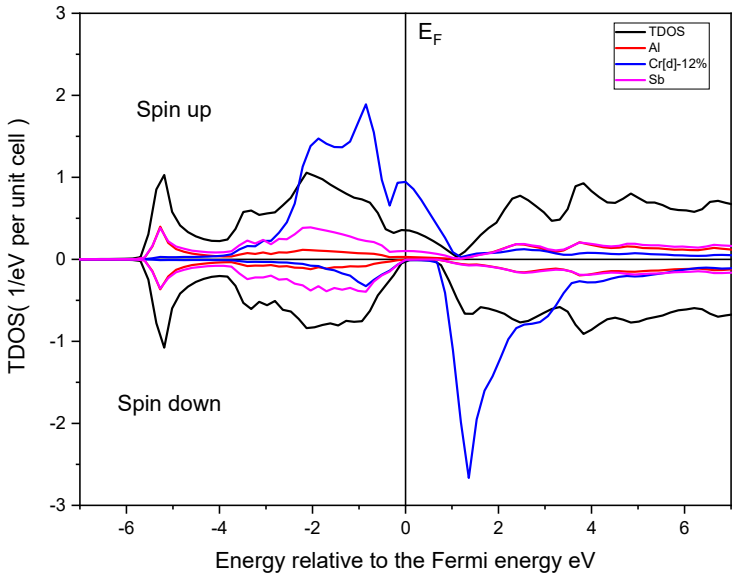

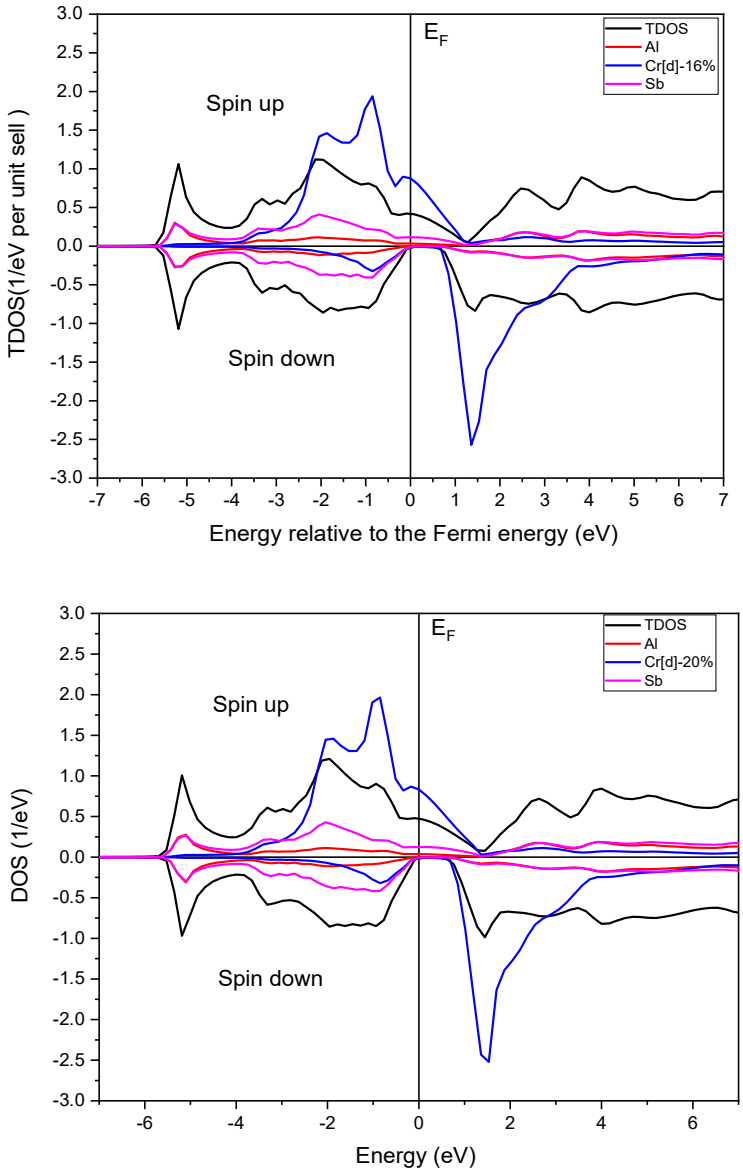

Figure 2. Total density of state (TDOS) and orbital projected density of state (PDOS) of substituted materials $Al_{1-x}Cr_xSb$ with x running from 4% to 20%.

To investigate the stability of the magnetic state in the system, we performed calculations to determine the energy of the system in two different magnetic configurations. The first configuration is ferromagnetic (FM), with all spins oriented in the same direction ($Al_{up1-x}Cr_{upx}Sb$).

The second configuration is the disordered local moment (DLM), also known as spin glass, where half of the transition metal impurity ion spins are oppositely oriented ($Al_{1-x}Cr_{upx/2}Cr_{dnx/2}Sb$). The energy difference between the two states, known as $\Delta E = E_{DLM} - E_{Ferro}$, has been calculated to study the stability of magnetic states [50, 51]. Furthermore, we estimated the Curie temperature of $Al_{1-x}Cr_xSb$ using the mean-field approximation (MFA), x represents the Cr concentration.

$$Tc = \frac{2}{3K_B}\frac{\Delta E}{x}$$

In this equation *KB* is the Boltzmann constant. The energy difference between the two states estimated for the exchange interaction and its values are displayed in Table 1.

It is evident from the table that as the amount of chromium in the material increases, it retains its ferromagnetic properties. Moreover, with a higher Cr content, the total magnetization also increases.

Table 1. The total energy differences, Stability Phases, Total and Local Moments for Cr Doped AlSb.

Cr%	ΔE (meV)	Stability phases	M^{Tot} (μB)	M^{Al} (μB)	M^{Cr} (μB)	M^{Sb} (μB)
4	0.00026	Ferro	0.11671	0.00163	3.13973	-0.02824
8	0.00146	Ferro	0.23694	0.00338	3.1305	-0.05262
12	0.00313	Ferro	0.35691	0.00504	3.12125	-0.07593
16	0.00517	Ferro	0.47674	0.00663	3.11375	-0.09868
20	0.00753	Ferro	0.59647	0.00817	3.10763	-0.12114
24	0.00095	Ferro	0.71616	0.00969	3.10249	-0.14348

Furthermore, Figure 3 shows the configuration of Cr-doped AlSb, which exhibits a positive ΔE, indicating that it is more stable in the ferromagnetic state than in the antiferromagnetic state. The analysis in Figure 3 shows that not only the 3d states of impurities but also the 4p states of Sb contribute significantly to the Fermi level. Co-doping of AlSb and Cr indicates that ferromagnetic stabilization is based on a double exchange mechanism with strong p-d hybridization. In addition, Figure 3 shows the calculated Curie temperature (TC) of Cr-doped sphalerite AlSb. The results show that both transition metals have high TC values above room temperature. Remarkably, the TC of vanadium is higher than that of titanium, reaching 750 K. Moreover, the figure shows that TC increases with doping concentration.

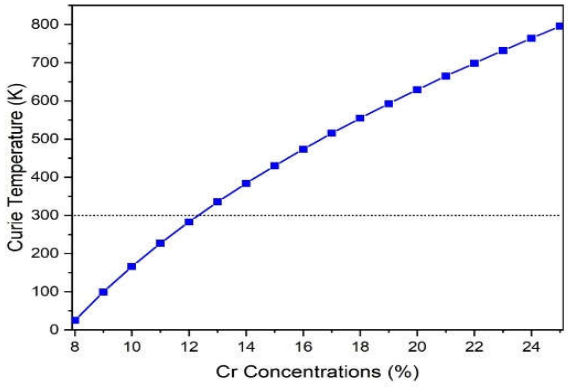

Figure 3. The calculations of Curie temperature for Cr-doped zinc-blende AlSb.

When compared to the reported alloys, $Yb_{14}MnSb_{11}$ [23] exhibits similar ferromagnetic properties as those observed in the examined Cr-doped AlSb and the ferromagnetic behavior of Ni-Mn-Sb [24].

CONCLUSION

Finally, we investigated the electronic and magnetic behavior of the AlSb alloy as a function of changing the chromium concentration. This work shows that DMO becomes a stable metalloid compound when the Cr element is incorporated as an impurity in AlSb. It also induces a ferromagnetic phase in the material. Due to the large value of magnetic moment, Cr is the main contributor to the magnetism of the system. TC is higher than room temperature and increases with Cr concentration, reaching a value of 740 K at 25%. Such materials are useful and are expected to have a great impact on the field of spintronics.

REFERENCES

1. Gupta, S.; Feng, L.J.; Medwal, R.; Vas, J.V.; Mishra, G.R.; Deen, M.; Paul, L.C.K.; Rawat, R.S. Spin-casted (Gd–Zn) co-doped $BiFeO_3$ thin films for sustainable oxide-electronics. *Mater. Sci. Semicond. Process.* **2021**, 132, 105902
2. Papaioannou, E.T.; Beigang, R. THz spintronic emitters: a review on achievements and future challenges. *Nanophotonics* **2021**, 10, 1243-1257.
3. Ding, M.; Gu, Xi.; Guo, L.; Zhang, R.; Zhu, X.; Li, R.; Zhang, X.; Hu, W.; Sun, X. The prospects of organic semiconductor single crystals for spintronic applications. *J. Mater. Chem. C* **2022**, 10, 2507-2515
4. Ume, R.; Gong, H.; Tokranov, V.; Yakimov, M.; Sadana, D.; Brew, K.; Cohen, G.; Lavoie, G.; Schujman, S.; Beckmann, K. Crystallization properties of Al-Sb alloys for phase change memory applications. *ECS J. Solid State Sci. Technol.* **2021**, 10, 075008.
5. Wang, X.; Xue, W.; Zhang, Z.; Li, X.; Yin, L.; Chen, C.; Yu, B.; Sui, J.; Cao, F.; Liu, X.; Mao, J.; Wang, Y.; Lin, X.; Zhang, Q. Stabilizing the optimal carrier concentration in Al/Sb-codoped GeTe for high thermoelectric performance. *ACS Appl. Mater. Interfaces* **2021**, 13, 45717-45725
6. Åberg, D.; Erhart, P.; Williamson, A.J.; Lordi, V. Intrinsic point defects in aluminum antimonide. *Phys. Rev. B* **2008**, 77, 165206.
7. Xia, Y.; Liu, B.; Wang, Q.; Zhang, Z.; Song, S.; Song, Z.; Yao, D.; Xi, W.; Guo, X.; Feng, S. Study on the phase change material Cr-doped Sb3Te1 for application in phase change memory. *J. Non-Cryst. Solids* **2015**, 422, 46-50.
8. Maftouh, A.; Rami, R.; Drissi, L.B.; El Fatni, O. ; Laamara, R. First-principles calculations for studying effect of tellurium (Te) doping on electronic properties, half-metallic ferromagnetism and “Curie temperature of V-doped AlSb DMS compound. *Solid State Commun.* **2021**, 339, 114482.
9. Rahman, G.; Cho, S.; Hong, S.C. Half metallic ferromagnetism of Mn doped AlSb: A first principles study. *Basic Solid State Phys.* **2007**, 244, 4435-4438.
10. Li, Z.; Li, J.; Wang, W.; Yan, Q.; Zhou, Y.; Zhu, L.; Cao, B.; Wei, B. Near zero-threshold voltage P-N junction diodes based on super-semiconducting nanostructured Ag/Al arrays. *Adv. Mater.* **2023**, 35, 2210612.
11. Qiu, P.; Yang, J.; Huang, X.; Chen, X.; hen L. Effect of antisite defects on band structure and thermoelectric performance of ZrNiSn half-Heusler alloys. *Appl. Phys. Lett.* **2010**, 96, 152105.
12. Baggetto, L.; Marszewski, M.; Gorka, J.; Jaroniec, M.; Veith, G.M. AlSb thin films as negative electrodes for Li-ion and Na-ion batteries. *J. Power Sources* **2013**, 243, 699.

13. Pino, R.; Ko, Y.; Dutta, P.S. Adhesion-free growth of AlSb bulk crystals in silica crucibles. *J. Cryst. Growth* **2006**, 290, 29.
14. Chen, W.T. Preparation and characterization of a gadolinium compound with high thermal stability. *Bull. Chem. Soc. Ethiop.* **2020**, 34, 479-488.
15. Sreedevi, R.; Joy Sinthiya, A.S.I.; Beaula, J.; Balu, T.; Murugakoothan, P. Growth, characterization and chemical computations of guanidinium trichloroacetate (GTCA) single crystal – DFT approach. *Bull. Chem. Soc. Ethiop.* **2023**, 37, 1033-1045.
16. Sani, S.; Tajo, Siraj, I.; Atiku Kurawa, M.; Abdul Halim, N.S. An efficient synthetic route, characterization and antimicrobial evaluation of Co(II), Ni(II), Cu(II) and Zn(II) Schiff base complexes. *Bull. Chem. Soc. Ethiop.* **2022**, 36, 801-813.
17. Sasaki, S.; Kusakabe, K.; Geshi, M.; Nagara, H.; Suzuki, N. First-principles electronic structure calculation of $LaCo_2$ in $MgCu_2$ structure. *J. Phys. Soc. Jpn.* **2007**, 76, 084711.
18. Rkhioui, N.; Tahiri, N.; Bounagui, O.E.; Ahl Laamara, R.; Drissi, L.B. Magnetism electronic and magnetic properties of CeO_2 doped with double impurities (Pd, C). *Mater. Res. Express* **2016**, 30, 165.
19. Rami, R.; Rkhioui, N.; Ahl Laamara, R.; Drissi, L.B. Electronic and magnetic properties of TiO_2 (co)-doped with (V, Mn). *Mater. Res. Express* **2017**, 4, 126513.
20. Akai, H. Department of Physics, Graduate School of Science, Osaka-University, Machikaneyama 1-1, Toyonaka, **2002**, 560-0043.
21. Salmani, E.; Benyoussef, A.; Ez-Zahraouya, H.; Saidi, E.H.; Mounkachi, O. First-principles study and electronic structures of Mn-doped ultrathin ZnO nanofilms. *Chin. Phys. B* **2012**, 21, 106601.
22. Das, S.; Ghosh, B.; Hussain, S.; Bhar, R.; Pal, A.K. Pulsed laser deposition: A viable route for the growth of aluminum antimonide film. *J. Cryst. Growth* **2015**, 419, 12.
23. Yang, X.; Pan, J.; Liu, S.; He, X.; Yang, M. Three-dimensional critical behavior and magnetocaloric effect in $Yb_{14}MnSb_{11}$. *J. Magn. Magn. Mater.* **2023**, 582, 170982.
24. Barman, R.; Kaur D. Improved magnetocaloric effect in magnetron sputtered Ni–Mn–Sb–Al ferromagnetic shape memory alloy thin films. *Vacuum* **2015**, 120, 22-26.